Kamil Maciuk*, Inese Vārna, and Chang Xu

Characteristics of seasonal variations and noises of the daily double-difference and PPP solutions

https://doi.org/10.1515/jag-2020-0042 Received October 6, 2020; accepted November 17, 2020

Abstract: Long term GNSS observations provided by networks of the continuously operating reference stations (CORS) allow for determination of the global and local tectonic plate movements and seasonal variations. In recent years, PPP (Precise Point Positioning) technique has become increasingly popular and most likely in the future will replace relative positioning with CORS stations. In this paper, we discuss the difference of the velocity and seasonal component estimates of 25 Latvian CORS stations on the basis of daily PPP solutions from the Nevada Geodetic Laboratory and double-difference solutions from the Institute of Geodesy and Geoinformatics of the University of Latvia. Time series of each coordinate component for 9-year time period were determined by the usage of the Tsview software and seasonal existence of linear, annual, semi-annual factors and their uncertainties were determined. Breaks (e.g., antenna and receiver changes) were also taken into account. We then assessed the noise characteristics of these time series with the use of overlapping Hadamard variance (OHVAR). The result shows that OHVAR is computationally cheap, and the dominating power-law noise, including flicker and random walk. However Hadamard deviation of the PPP and double-difference solutions scatters differently for a whole year averaging time due to the different GNSS data strategies.

Keywords: CORS, overlapping Hadamard variance, noise, PPP, time series

https://orcid.org/0000-0001-5514-8510

Inese Vārna, Institute of Geodesy and Geoinformatics, University of Latvia, Jelgavas street 3, LV-1004, Riga, Latvia, e-mail: inese varna@lu.lv

Chang Xu, School of Road and Bridge, Zhejiang Institute of Communications, No. 1515, Moganshan Road, Hangzhou, Zhejiang Province, 311112, P.R. China, e-mail: xuchang404@163.com

1 Introduction

Continuous GNSS (Global Navigation Satellite System) time series has been extensively used in Earth surface motion monitoring (e.g., plate tectonics [1, 2], sea-level variation [3, 4], polar research [5] and other [6, 7]). Multi-year combination dense GNSS network solutions of the EPN weekly SINEX files [8] play an important role in providing accurate stations' positions and velocities in the European territory. Since the BIFROST (Baseline Inferences for Fennoscandian Rebound Observations Sea Level and Tec-tonics) project [9] was initiated in 1993, a number of works [10, 11, 12] have been concerned with measuring the crustal deformation rates in Fennoscandia and establishing insight into physics of the GIA (glacial isostatic adjustment) response. Notably territory of Latvia, which is located on the border of an area that is exposed to longterm intra-continental deformations in response to GIA of Fennoscandia, has been receiving more attention in recent years. Attempts to characterise land uplift effect in Latvia by analysing precise levelling data have been made earlier [13, 14]. Latvian continuously operating reference station (CORS) rates (or velocities) has been previously analysed [15, 16] and have shown that GIA effect rates up to about 2 mm/yr in the vertical direction in the north-western part of Latvia. However, no detailed analysis of seasonal variations and noise characteristics of the Latvian CORS have been performed up till now. Modelling seasonal variations and noise in coordinate time series is important for reliable estimation of CORS station velocities and their uncertainties [17]. As such, further assessment of the noise characteristics in Latvian CORS coordinate time series and then discussion of the velocity and seasonal variations as well as their uncertainties is still a meaningful task.

Many literature sources [18, 19, 20] reveal that the maximum likelihood estimation (MLE) method which using a data covariance incorporates a variety of noise processes is the most popular and rigorous approach to detection of noise contents in geodetic time series. Many noise models (including autoregressive and moving average noise, power-law, flicker noise (FL), random walk noise (RW), white noise (WH) and Generalized Gauss Markov noise) are found in the GNSS coordinate time series both in regional and global networks. If neglecting this coloured

^{*}Corresponding author: Kamil Maciuk, Department of Integrated Geodesy and Cartography, AGH University of Science and Technology, Mickiewicza Av 30, 30-059 Krakow, Poland, e-mail: maciuk@agh.edu.pl, ORCID:

noise, the uncertainty of site velocity could be underestimated by a factor of 2-4 [19, 21]. However the main disadvantage of MLE is the fact that it is a computationally demanding and it may be affected by the strongest noise while evaluating a combined noise model [22]. RW is consequently difficult to be accurately determined in a short time series since the flicker noise is often dominated and masking RW [19]. Recently, Allan variance, an efficient algorithm that is often used to assess the atomic oscillators stability, is introduced into many geodetic applications. Malkin and Voinov [23] first adopted Allan variance to process the site coordinates of the European GNSS network EUREF. Niu et al. [24] used Allan variance to measure the error characteristics of GNSS PPP (Precise Point Positioning) solutions. Hackl et al. [25] reveal that Allan variance is an alternative and accurate method to estimate the rate uncertainty for South African TrigNet network. Due to the good confidence in dealing with divergent noise, Xu and Yue [26] adopted a modified Allan variance approach called overlapping Hadamard variance (OHVAR) to infer the noise components of daily PPP position time series of 12 International GNSS Service (IGS) sites in China. They found that the dominate power-law noise inferred by OHVAR agrees well with that inferred by MLE. These previous works greatly inspire our research to extend the use of Allan deviation (and related) to further assess the noise characteristics of the Latvian CORS stations.

The rest of the article is organized as follows. Section 2 describes the selected Latvian CORS and the *Tsview* software, a program packaged with the GAMIT/GLOBK software suite used to analyse GNSS data. OHVAR is also briefly outlined. Section 3 describes the GNSS data included in this study. Section 4 discusses site velocity and seasonal variation estimates for PPP and double-difference (DD) solutions. Noise characteristics of the Latvian CORS stations are investigated. Section 5 presents final remarks.

2 Materials and methods

In Latvia, there are two CORS networks – LatPos, EUPOS®-Riga; and EUREF Permanent GNSS Network (EPN) station RIGA. In this study 25 Latvian CORS stations (24 LatPos stations and EPN station RIGA) (see Figure 1) were analysed. LatPos network covers all territory of Latvia and is under the supervision of Latvian Geospatial Information Agency. This network is operating since 2006/2007 and most of the stations are installed on the roofs of brick

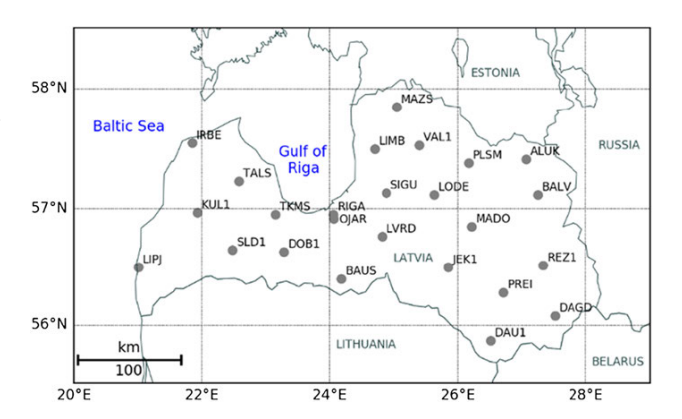


Figure 1: Latvian CORS selected for the study.

or concrete buildings. LatPos network has evolved significantly during those years – 18 stations were operating in 2007, for most of the station's antennas and/or receivers have been changed, numerous stations have been moved to other locations, 8 new stations were installed. All stations are equipped with Leica GNSS receivers and antennas.

All receivers, antennas and their changes for analysed stations during 2011-2019.6 are listed in Table 1.

The data coverage for analysed stations is shown in Figure 2. Starting with the end of 2019 LatPos is experiencing further improvements – switch to antennas and receivers with Galileo capability for all stations and movement to other sites for most of the stations. However, Nevada Geodetic Laboratory (NGL) contains LatPos data just till mid-August 2019, therefore the time series adopted in this study does not cover the last changes of the network. Stations were selected considering the length of the time series – longer than 5 years, therefore LatPos stations VALK operating since 2015, VAIN – since 2016, KUL2 – since 2017, LIP2, LVR1 and MAZ2 – since 2018 were not analysed.

However, the analysis of the selected time series may be affected by numerous factors. Receiver and antenna changes are shown in Table 1. Station LVRD has been affected since 2017 when air ventilation system was installed near the antenna and caused obvious scatter in coordinate time series. Additional breaks caused by unknown reasons were identified for stations KUL1, LODE and PREI. Main mount type is either 20 or 200 mm diameter metal pipe, either 1 or 1.5 m high, located on the roofs of stable concrete or brick buildings, except stations OJAR and TKMS with mount height 2 m, station SLD1 with mount height 3 m, stations DOB1 and LIMB with mount height 5 m, stations IRBE and RIGA mounted on grounded concrete pillar, station MAZS mounted on grounded 8 m high steel mast.

Table 1: Receivers, antennas and their changes for LatPos network and RIGA station during 2011-2019.6.

Station	Receiver	Antenna
ALUK	2019-07-17 LEICA GRX1200+GNSS → LEICA GR30	LEIAR25LEIT
BALV	2019-07-17 LEICA GRX1200+GNSS \rightarrow LEICA GR 30	2014-06-12 LEIAT504 LEIS \rightarrow LEIAR20 LEIM
BAUS	2013-02-27 LEICA GRX1200PRO \rightarrow LEICA GRX1200+GNSS	LEIAT504 LEIS
DAGD	2017-11-10 LEICA GRX1200+GNSS \rightarrow LEICA GR30	2018-03-07 LEIAT504 LEIS \rightarrow LEIAR20 LEIM
DAU1	2011-02-02 LEICA GRX1200PRO $ ightarrow$ LEICA GRX1200+GNSS	LEIAT504 LEIS
DOB1	LEICA GRX1200+GNSS	LEIAT504 LEIS
IRBE	2019-07-03 LEICA GRX1200+GNSS \rightarrow LEICA GR 30	LEIAR25 LEIT
JEK1	2019-07-18 LEICA GRX1200+GNSS \rightarrow LEICA GR 30	LEIAR25 LEIT
KUL1	LEICA GRX1200+GNSS	LEIAT504 LEIS
LIMB	LEICA GRX1200+GNSS	LEIAT504 LEIS
LIPJ	LEICA GRX1200+GNSS	LEIAT504 LEIS
LODE	2019-07-18 LEICA GRX1200+GNSS \rightarrow LEICA GR 30	2014-06-03 LEIAT504 LEIS → LEIAR20 LEIM
LVRD	LEICA GRX1200+GNSS	2011-09-14 LEIAR25 NONE → LEIAR25 LEIT
MADO	LEICA GRX1200+GNSS	LEIAT504 LEIS
MAZS	LEICA GRX1200+GNSS	LEIAX1202GG NONE
OJAR	2012-01-02 LEICA GRX1200GGPRO $ ightarrow$ LEICA GR10	LEIAR25 LEIT
	2018-01-31 LEICA GR10 $ ightarrow$ LEICA GR30	
PLSM	2013-03-27 LEICA GRX1200PRO \rightarrow LEICA GRX1200+GNSS	LEIAT504 LEIS
PREI	2011-01-27 LEICA GRX1200PRO $ ightarrow$ LEICA GRX1200+GNSS	LEIAT504 LEIS
	2014-02-12 LEICA GRX1200+GNSS \rightarrow LEICA GRX1200GGPRO	
	2014-03-12 LEICA GRX1200GGPRO \rightarrow LEICA GRX1200+GNSS	
	2014-05-14 LEICA GRX1200+GNSS \rightarrow LEICA GRX1200+GNSS	
REZ1	LEICA GRX1200+GNSS	LEIAR25 LEIT
RIGA	2013-12-11 LEICA GRX1200PRO $ ightarrow$ LEICA GR25	2013-12-11 LEIAT504 LEIS → LEIAR25.R4 LEIT
SIGU	LEICA GRX1200+GNSS	LEIAT504 LEIS
SLD1	LEICA GRX1200+GNSS	LEIAT504 LEIS
TALS	LEICA GRX1200+GNSS	LEIAT504 LEIS
TKMS	2014-02-08 LEICA GRX1200GGPRO $ ightarrow$ LEICA GRX1200+GNSS	LEIAR10 NONE
	2018-04-25 LEICA GRX1200+GNSS \rightarrow LEICA GR10	
VAL1	LEICA GRX1200+GNSS	LEAT504 LEIS

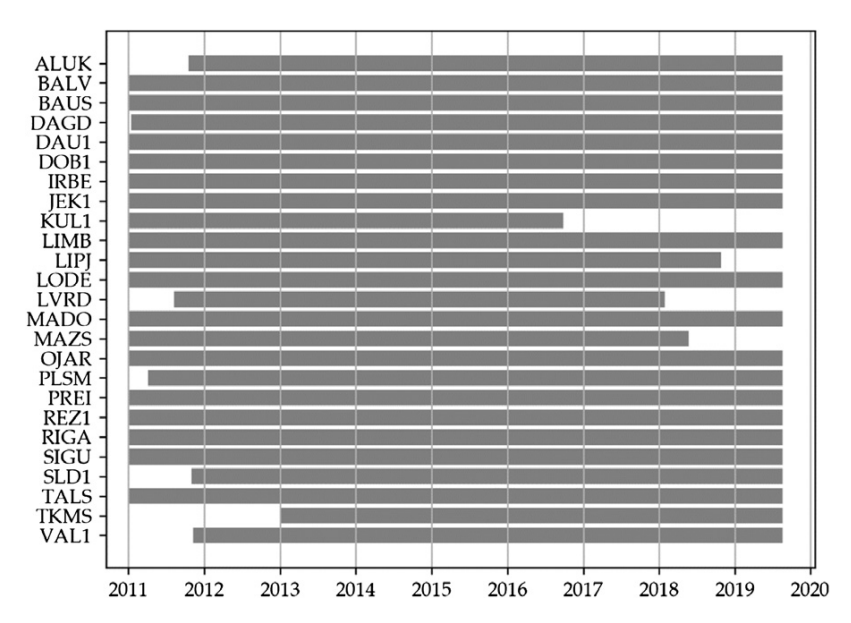


Figure 2: Data coverage of Latvian CORS during 2011-2019.6.

Station MAZS was exceptionally negatively affected by its mount type and as it will be seen in the results.

Tsview software is based on least-squares fitting and complemented in the GAMIT/GLOBK software package [27]. The time series are analysed according to commonly used time-dependent functional model [28]:

$$y(t_{i}) = y_{0} + bt_{i} + \sum_{f=1}^{2} \{c_{f} \sin 2\pi f t_{i} + d_{f} \cos 2\pi f t_{i}\}$$
$$+ \sum_{i=1}^{n_{g}} g_{j} H(t_{i} - T_{j}) + \varepsilon_{y}(t_{i}), \qquad (1)$$

where $v(t_i)$ is the initial position at the reference epoch $t = t_i$ (unit – year), y_0 and b are the position (t = 0) and velocity parameters, c_f and d_f are the periodic motion parameters (f = 1, 2 represent the annual and semi-annual seasonal terms). The offsets term $\sum_{j=1}^{n_g} g_j H(t_i - T_j)$ is caused by antenna or receiver changes, reposition of station and other known or unknown human intervention events, gi is the magnitude of the offset at epoch T_i , n_g is the total number of offsets and H is the Heaviside step function. $\varepsilon_{\nu}(t_i)$ represents the noise term. The unknown parameters that are estimated during least-squares fitting according to Eq. (1) with *Tsview* are y_0 , b, c_f , d_f and g_i . The uncertainties of parameters in Tsview are estimated using the Real Sigma algorithm [27] which is a time-correlated noise model assuming that the noise process is a first-order Gauss Markov process. Outliers were removed using the 3σ criterion.

Statistically variance σ^2 is expressed as a mean of squares differences between respective data x_i and their mean value \overline{x} for a n number of data:

$$\sigma^2 = \frac{1}{n} \sum_i (x_i - \overline{x})^2 \tag{2}$$

Standard deviation is a square root of the variance. The *i*th average deviation over an interval τ (called interval of averaging or averaging time) of a finite set of x data:

$$\overline{y}_i = \frac{x_{i+1} - x_i}{\tau} \tag{3}$$

with assumption that two time deviation measurements are spaced τ apart. Allan variance for a finite set of the data is expressed as follows [29]:

$$\sigma_y^2(\tau) = \frac{1}{2} (\bar{y}_{i+1} - \bar{y}_i)^2$$
 (4)

Combination of equations (3) and (4) leads to:

$$\sigma_y^2(\tau) = \frac{1}{2\tau^2(N-2)} \sum_{i=1}^{N-2} (x_{i+2} - 2x_{i+1} + x_i)^2$$
 (5)

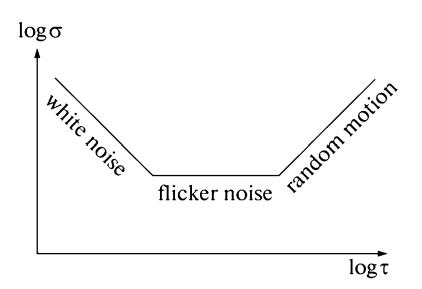


Figure 3: The graphical determination of the type of the noise component of the signal by AVAR σ^2 , calculated for different intervals of averaging τ [32].

where N is a finite the number of data spaced by the measurement interval τ .

Hadamard variation is more efficient than Allan variance due to its insensitivity to linear frequency drift. Hadamard variance is defined as follows [30]:

$$H\sigma_y^2(\tau) = \frac{1}{6\tau^2(N-3)} \sum_{i=1}^{N-3} (x_{i+3} - 3x_{i+2} + 3x_{i+1} - x_i)^2$$
 (6)

where $\tau = m\tau_0$, m is an averaging factor and τ_0 is the basic measurement interval.

The OHVER is a modification of the Hadamard variance, which makes a maximum use of the data set by forming a possible fully overlapping samples at each averaging time. OHVER can provide a better confidence than Allan variance and Hadamard variation [31]. For a frequency data OHVAR is defined as [30]:

$$OH\sigma_{y}^{2}(\tau) = \frac{1}{6m^{2}(M - 3m + 1)} \sum_{j=1}^{M - 3m + 1} \sum_{i=1}^{j+m-1} (y_{i+2m} - 2y_{i+m} + y_{i})^{2}$$
(7)

Allan variance (and related) is connected with averaging time as:

$$\sigma_y^2(\tau) \sim \tau^{\mu} \tag{8}$$

where μ characterizes the type of noise present in the time series. Allan variance (and related) figures are displayed in as log-log plots and dominating noise processes at different averaging intervals (τ) are determined by means of the slopes (see Figure 3).

3 Data

In this study daily coordinate time series based on both PPP and DD solutions are considered. The PPP coordinate time series from NGL are processed using the

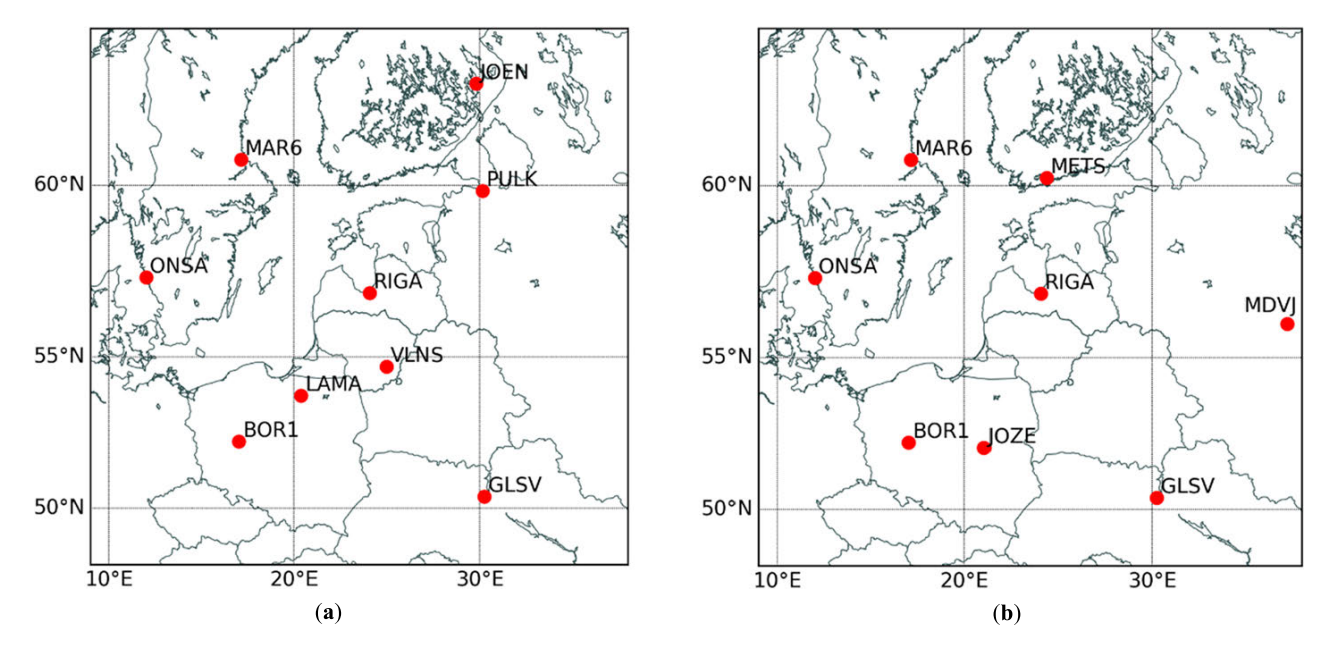


Figure 4: IGS/EPN stations used as reference stations: (a) in the reference frame IGb08; (b) in the reference frame IGS14.

GIPSY/OASIS-II software [33]. The Wet and Dry interpolated components from the Vienna Mapping Function VMF1 was used as the a priori troposphere model. Zenith delay and gradients are estimated as random every 5 minutes. A cut-off elevation angle of 7° was selected. The 1st order ionosphere effect is removed by LC and PC combinations, and 2nd order effect is modelled using IONEX data with IGRF12. Solid Earth tides, ocean tidal loading and Earth rotation have been applied according to IERS 2010 Conventions in the primary data processing, whereas nontidal (e. g., atmospheric and surface hydrological) loadings are not yet taken into account in the processing. More details about the GNSS data analysis strategy can be found on the website http://geodesy.unr.edu/gps/ngl.acn.txt.

Institute of Geodesy and Geoinformatics of the University of Latvia (GGI) is contributing as an EPN Densification analysis centre, by regularly transferring weekly SINEX solutions to EPN. The DD solutions have been computed for the 8.6 year period from 2011 to 2019.6 by using the Bernese GNSS Software v5.2 [34]. The final CODE (Center for Orbit Determination in Europe) precise orbits, Earth orientation and clock products, and CODE final ionosphere product were used for GNSS data processing. The dry Global Mapping Function was used as the a priori troposphere model, while zenith path delay parameters were estimated using the wet Global Mapping Function. A cutoff elevation angle of 3° was selected. The positions of all stations were corrected for both solid Earth tide effect, and ocean tide loading. Nine IGS/EPN stations: BOR1 (Poland), GLSV (Ukraine), JOEN (Finland), LAMA (Poland), MAR6 (Sweden), ONSA (Sweden), PULK (Russia), RIGA (Latvia), VLNS (Lithuania), with the minimum constrained coordinates and velocities were used as reference stations in the reference frame IGb08 (see Figure 4a).

Since January 29, 2017, 8 IGS/EPN stations: BOR1 (Poland), GLSV (Ukraine), JOZE (Poland), MAR6 (Sweden), MDVJ (Russia), METS (Finland), ONSA (Sweden), RIGA (Latvia), with the minimum constrained coordinates and velocities were used as reference stations in the reference frame IGS14 (see Figure 4b).

4 Results and discussion

We first visually inspect the residual time series by using *Tsview*. This step is necessary to detect offsets and station misbehaviour. For example, station MAZS which was mounted on an 8 m high steel mast, has the highest amplitude of the residual signal. The station horizontal and vertical velocities and their uncertainties were estimated for both NGL-PPP and GGI-DD coordinate time series. NGL-PPP solutions are available in ETRF2014 and ITRF2014. GGI-DD daily coordinate solutions were also expressed in ETRF2014 and ITRF2014 using ITRF2008-to-ETRF2014, ITRF2008-to-ITRF2014 and ITRF2014-to-ETRF2014 one-step transformation with 14 transformation parameters according to [35]. Figure 5 provides the station horizontal and vertical velocities of NGL-PPP and GGI-DD solutions (in ETRF2000 and ITRF2008 reference frames) for the

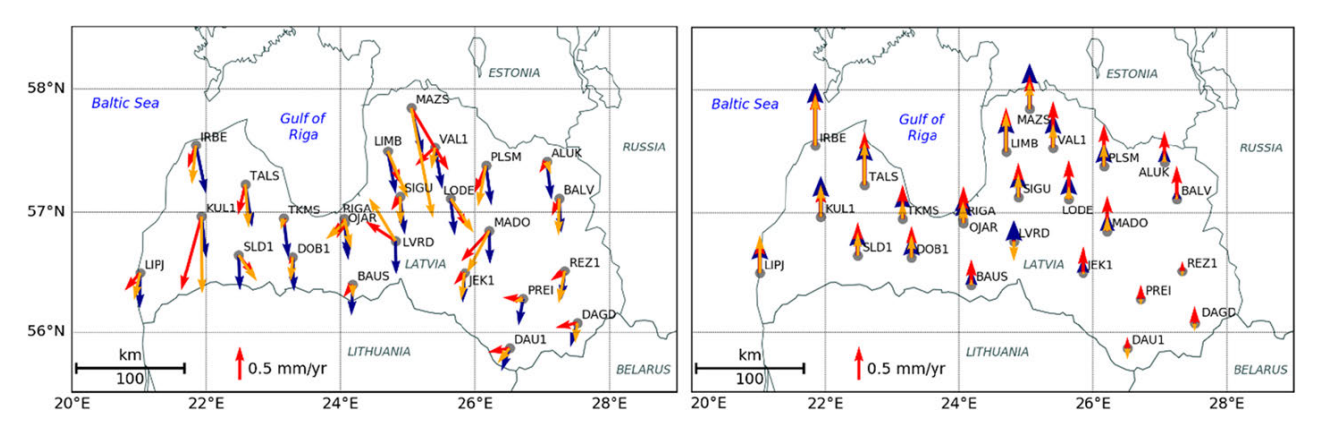


Figure 5: Latvian CORS station horizontal velocities in ETRF2000 (a) and vertical velocities in ITRF2008 (b); NKG velocity models – blue; GGI-DD solution – red, NGL-PPP solution – orange.

Table 2: Mean STDV and RMS of NGL-PPP velocity differences (mm/yr) from the GGI-DD velocities.

	NGL-PPP vs. GGI DD, ETRF2014			NGL-PPP vs. GGI-DD, ITRF2014		
	North	East	Up	North	East	Up
Mean	0.43	0.52	-0.44	-0.17	0.08	-0.49
STDV	0.15	0.12	0.26	0.19	0.12	0.27
RMS	0.45	0.53	0.51	0.25	0.14	0.56

8.6-year observation period, as well as NKG (Nordic Geodetic Commission) velocity models (i. e. NKG_RF03vel [36] and NKG2016LU_abs [37]). We noted that the MIDAS (Median Inter-annual Difference Adjusted for Skewness) [38] may not be suitable for multi velocity solution and stations with large post-earthquake relaxation deformation, so the NGL velocities estimated by MIDAS were tentatively not considered here.

Table 2 and Table 3 give the velocity inconsistency among NGL-PPP, GGI-DD and NKG's velocity models. In order to compare NGL-PP and GGI-DD solutions to NKG models the horizontal velocities were expressed in the ETRF2000 frame and the velocities for the vertical (hereafter – Up) component in the ITRF2008. The velocity inconsistency between NGL-PPP and GGI-DD is: 0.43 \pm 0.15 mm/yr for North, 0.52 \pm 0.12 mm/yr for East and 0.44 \pm 0.26 mm/yr for Up components in ETRF2014; 0.17 \pm 0.19 mm/yr for North, 0.08 \pm 0.12 mm/yr for East and 0.49 \pm 0.27 mm/yr for Up components in ITRF2014. The results reveal that horizontal components agree better in ITRF2014 and slightly better for Up component in ETRF2014.

Comparison of GNSS solutions with NKG models shows that NGL-PPP has slightly better agreement with NKG_RF03vel model while GGI-DD solution has systematic shift with compared NKG_RF03vel model for horizontal components. Meanwhile, GGI-DD has a slightly better

agreement with NKG2016LU_abs model for Up component. Additionally, *Tsview* estimated mean velocity uncertainties are: vertical 0.18 mm and horizontal 0.08 mm for GGI-DD; vertical 0.17 mm and horizontal 0.06 mm for NGL-PPP. Recall that the uncertainties may be too optimistic since the default noise assuming in *Tsview* is a first-order Gauss Markov process.

Figure 6 gives the amplitude estimates of sine and cosine function for both NGL-PPP (left) and GGI-DD (right) in ETRF frame. For the best understanding of the size in the figure below, the scales for each component are the same. Amplitudes for all stations vary around 1 mm for horizontal components and Up component in GGI-DD solutions. In NGL-PPP solutions seasonal amplitudes are much more scattered, especially in Up component, where the amplitude reaches up to 4 mm for several stations. Moreover, there are stations in both PPP and DD solutions with extremely high amplitudes comparing to other stations. In both PPP and DD solutions North component for station MAZS is characterised by more than 2 and 3 mm higher amplitude in case of cosine and sine respectively. While for other stations North component amplitudes are less than 1 mm. In case of East component there are two stations with outlying amplitudes, for PPP technique these are BALV and SLD1 with values close to 2 mm, in case of DD these are PRE1 and SLD1 – also around 2 mm amplitude.

Table 3: Mean STDV and RMS of GGI-DD and NGL-PPP velocity differences (mm/yr) from the deformation models NKG_RF03vel (North, East) and NKG2016LU_abs (Up).

	GGI-DD vs. NKG_RF03vel, ETRF2000 (North, East); GGI-DD vs. NKG2016LU_abs, ITRF2008 (Up)			NGL-PPP vs. NKG_RF03vel, ETRF2000 (North, East); NGL-PPP vs. NKG2016LU_abs, ITRF2008 (Up)		
	North	East	Up	North	East	Up
Mean	0.25	-0.16	0.18	0.10	-0.05	-0.29
STDV	0.24	0.20	0.30	0.37	0.17	0.26
RMS	0.34	0.25	0.34	0.37	0.17	0.39

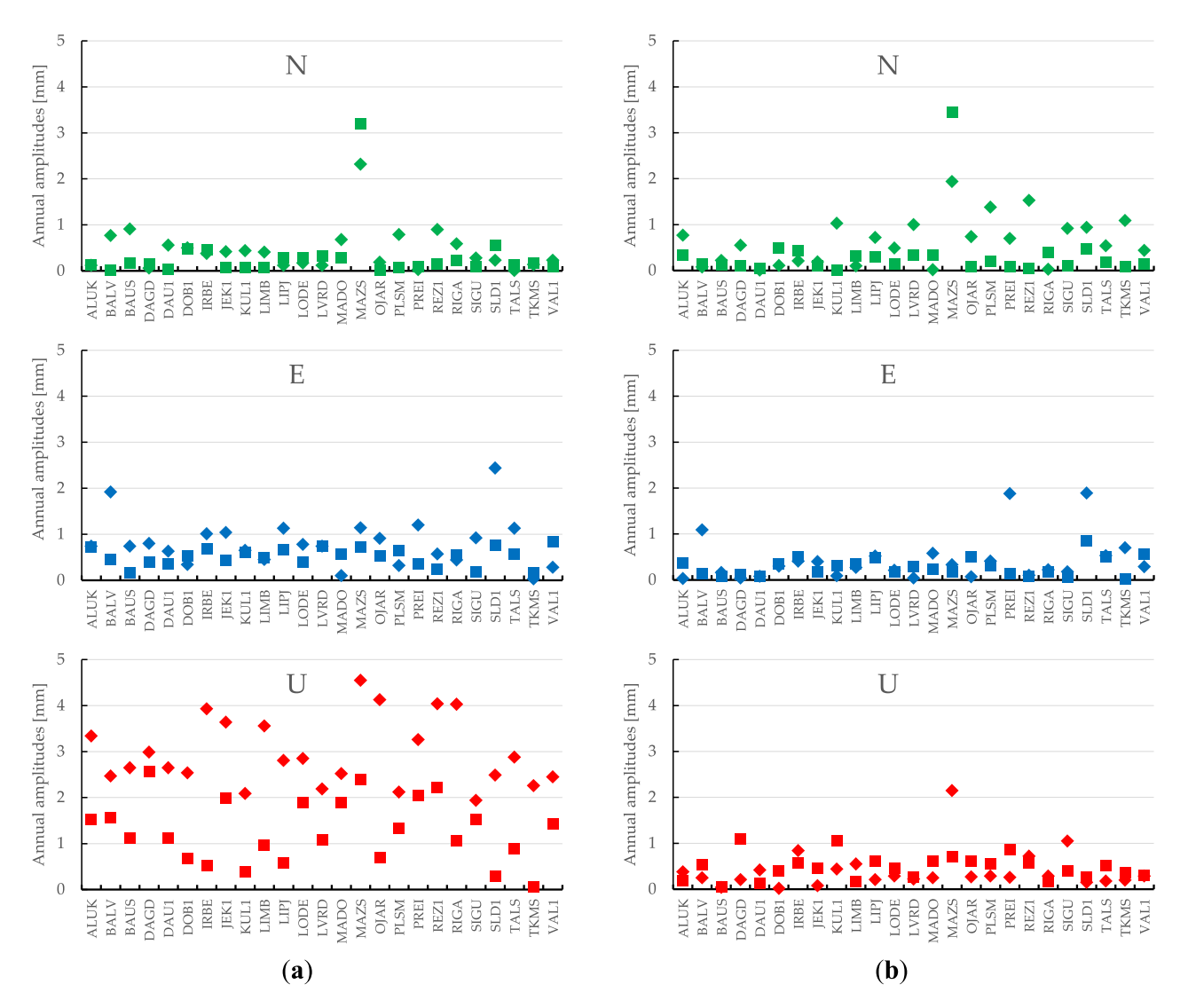


Figure 6: Annual sine (squares) and cosine (diamonds) amplitudes of NGL-PPP (a) and GGI-DD (b) function.

Up component amplitudes for GGI-DD results are at about 1 mm level (MAZS standing out with 2> mm cosine factor), but these results are consistent with each other. In case of NGL-PPP amplitudes are much bigger and have rather random size which varies from 1 mm to 4 mm. More-

over, MAZS amplitude is not as distinct as in the case of NGL-DD solutions, it is only slightly larger than several other stations with amplitudes larger than 4 mm values. Figure 7 shows PPP and DD coordinates time series of stations with the biggest amplitudes in each direction. In case

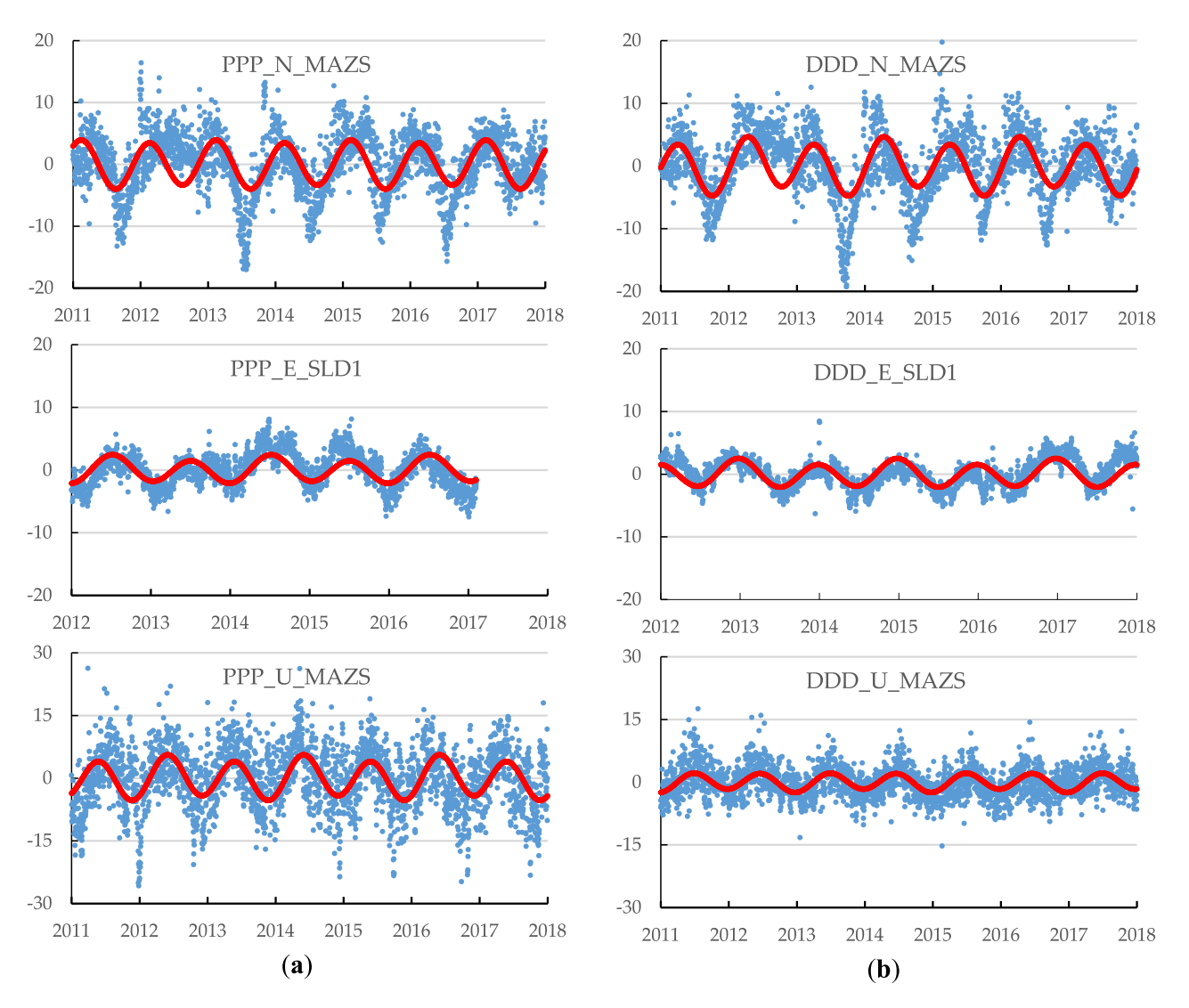


Figure 7: Coordinates components of two stations with the biggest amplitudes (blue) for the fitted function (red). Time scale in years presents x-axis; y-axis is an amplitude in mm, for North, East and Up direction respectively counting from the top.

of North component for each solution MAZS is typical of the biggest amplitude.

No correlation between the magnitude of seasonal amplitudes and the geographical location is found in this study. MAZS station has been installed on an 8 m high steel mast that might affect the occurrence of such large amplitude in North and Up directions. It stands out clearly against the other stations and it appears that its data quality is not acceptable for geodynamical studies. Also, station SLD1 has been installed on a 3 m high metal pipe that could cause apparent strong seasonal signal in East direction. All other stations are installed on 1, 1.5 or 2 m high metal pipes or more stable metal constructions, except DOB1 which is installed on a 5 m high metal pipe, however DOB1 does not show any significant seasonal behaviour.

Appendices A and B contain OHVAR calculated for all three components of the 25 stations based on NGL-PPP and GGI-DD position time series in the ITRF14 reference frame. We find it promising to detect dominant power-law noise in the time domain. In the case of the PPP time series (Appendix A) the slope of the power-law curve for the averaging time between 1 and 7 days is -0.621 and -0.613 for E and N components, respectively. This power-law curve presents a noise type close to WH. For the 1 to 30 day averaging time it becomes closer to FL, but still closest to WH (-0.309 for East and -0.405 for North component). For a whole year averaging time (1 to 365 days) curves become more flat, -0.155 and -0.275 for the E and N components, respectively. In the case of the Up component part of the stations' curves is characterized by unrecognized

noise type with a slope more than 2–3, which leads to 1.886 mean power-law curve for 1 to 7 days averaging time. For the longer averaging time, 1 to 30 days and 1 to 365 days it is described by RW noise with 0.992 and 0.275 values respectively. Similar power-law curves also indicate similar sources of noise for the majority of the sites.

Appendix B shows that DD solutions scatter differently for a whole year averaging time due to the different GNSS data processing strategy. For the 1 to 7 days averaging intervals, the slope of the power-law curve is -1.174 and -1.170 for East and North component respectively. For the longer averaging time (1 to 30 days) it is -0.692 for East and -0.748for North component, the power-law curve represents WH noise. For the 1 to 365 days averaging time, it becomes flatter with -0.264 and -0.252 values for E and N component, respectively. For the Up component, results differ significantly from PPP solution, for the 1 to 7 days and 1 to 30 days averaging time the slope of the power-law curve is 0.782 and 0.273, respectively which is close to RW noise. For the 1 to 365 days averaging time it becomes to be flat (-0.014 slope of the power-law curve), which is represented by the FL noise. Comparing component curves they are less consistent and correlate more closely with each other than with PPP solutions. In addition, these curves are characterized by a smaller number of time series standing-off from the other, as is the case with data obtained using the PPP technique.

5 Conclusions

PPP and double-difference GNSS time series of the 25 Latvian CORS stations were analysed in this paper. Analyses cover velocities, seasonality, stability and noises determination of the data. The results indicate the effect of the Fennoscandian rebound in the territory of Latvia. Inconsistent velocity uncertainties are found between DD and PPP solutions. Latvian CORS station vertical velocity vectors have maximum values in the north-western part of Latvia and minimum values in the south-eastern part of the country. We also find that NGL-PPP agrees slightly better with the NKG_RF03vel model, while GGI-DD has a shift with the NKG_RF03vel model in horizontal components. Meanwhile, GGI-DD agrees slightly better with the NKG2016LU_abs model for the Up component.

Some stations show significant seasonality effects with amplitudes bigger than expected coordinate's accuracy (1 mm for horizontal and 3 mm for Up component). There are only a couple of stations with seasonal function

amplitudes larger than 1 mm for horizontal components for DD solutions. In case of height amplitudes obtained from the PPP technique – due to lower accuracy than in the double-difference method – amplitudes for each station are bigger.

Overlapping Hadamard variance shows the existence of the WH noise as dominant in the horizontal component in early averaging time. In the case of the PPP for the longest averaging intervals for N and E components WH+FL combination is seen. In the case of the Up component for PPP solutions, RW noise is dominant in some sites. In the case of DD solutions, RW is dominant, and for the longest averaging interval dominant noise types are RW+FL. In addition, all time series are consistent with each other in terms of individual components, while this is more apparent with the relative solution than in PPP. Further research is needed to estimate reliable velocity uncertainties and validate noise types detected in this study by using MLE.

Author contributions: Kamil Maciuk -45%, Inese Vārna -40%, Chang Xu -15%.

Funding: This research was funded by grant number scientific research 16.16.150.545 and the National Natural Science Foundation of China (grant No. 41804007).

Appendix A

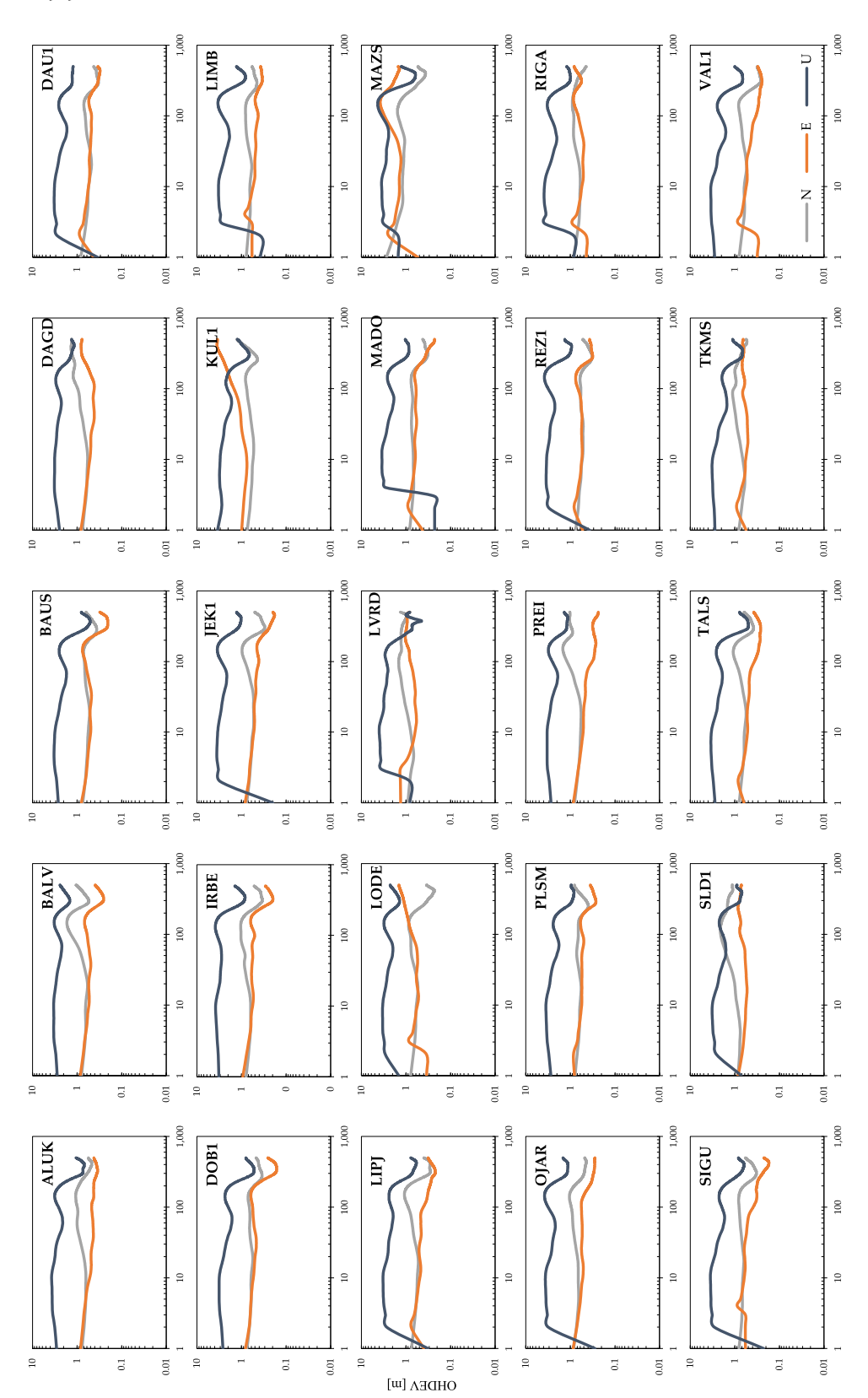


Figure 8: OHVAR of the NGL-PPP solutions.

Appendix B

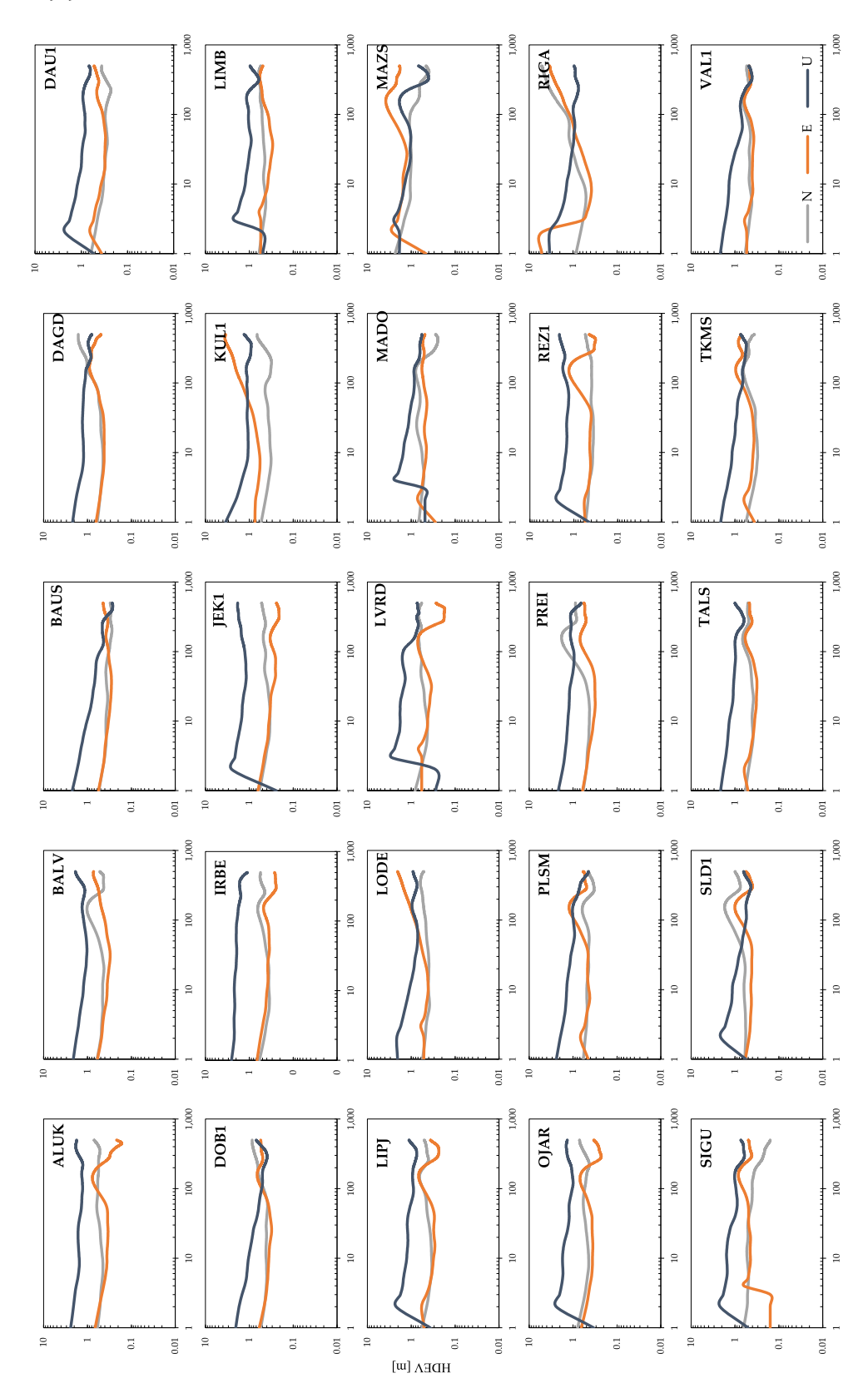


Figure 9: OHVAR of the GGI-DD solutions.

References

- [1] G. Blewitt and D. Lavallée, 'Effect of annual signals on geodetic velocity', J. Geophys. Res. Solid Earth, vol. 107, no. B7, pp. ETG 9-1-ETG 9-11, Jul. 2002.
- [2] A. R. Riddell, M. A. King, and C. S. Watson, 'Present-day vertical land motion of Australia from GPS observations and geophysical models', J. Geophys. Res. Solid Earth, vol. 125, no. 2, Feb. 2020.
- J. S. Löfgren and R. Haas, 'Sea level measurements using multi-frequency GPS and GLONASS observations', EURASIP J. Adv. Signal Process., 2014, no. 1, p. 50, 2014.
- [4] A. Santamaría-Gómez, C. Watson, M. Gravelle, M. King, and G. Wöppelmann, 'Levelling co-located GNSS and tide gauge stations using GNSS reflectometry', J. Geod., vol. 89, no. 3, pp. 241-258, Mar. 2015.
- P. Lewińska and P. Zagórski, 'Creating a 3D database of Svalbard's historical sites: 3D inventory and virtual reconstruction of a mining building at Camp Asbestos, Wedel Jarlsberg Land, Svalbard', Polar Res., vol. 37, no. 1, 1485416, Jan. 2018.
- S. Miura, S. Ueki, T. Sato, K. Tachibana, and H. Hamaguchi, 'Crustal deformation associated with the 1998 seismo-volcanic crisis of Iwate Volcano, Northeastern Japan, as observed by a dense GPS network', Earth, Planets Sp., vol. 52, no. 11, pp. 1003-1008, 2000.
- [7] A. Bieda, J. Bydłosz, A. Warchoł, and M. Balawejder, 'Historical underground structures as 3D cadastral objects', Remote Sens., vol. 12, no. 10, p. 1547, May 2020.
- [8] A. Kenyeres et al., 'Regional integration of long-term national dense GNSS network solutions', GPS Solut., vol. 23, no. 4, p. 122, Oct. 2019.
- 'GPS measurements to constrain geodynamic processes in Fennoscandia', Eos, Trans. Am. Geophys. Union, vol. 77, no. 35, p. 337, 1996.
- [10] H. P. Kierulf, H. Steffen, M. J. R. Simpson, M. Lidberg, P. Wu, and H. Wang, 'A GPS velocity field for Fennoscandia and a consistent comparison to glacial isostatic adjustment models', J. Geophys. Res. Solid Earth, vol. 119, no. 8, pp. 6613-6629, Aug. 2014.
- [11] M. Lidberg, J. Johansson, H.-G. Scherneck, G. Milne, and J. Davis, 'New Results Based on Reprocessing of 13 years Continuous GPS Observations of the Fennoscandia GIA Process from BIFROST', 2009, pp. 557-568.
- [12] J. M. Johansson, 'Continuous GPS measurements of postglacial adjustment in Fennoscandia 1. Geodetic results', J. Geophys. Res., vol. 107, no. B8, p. 2157, 2002.
- [13] M. Idžanović, C. Gerlach, K. Breili, and O. Andersen, 'An attempt to observe vertical land motion along the Norwegian coast by CryoSat-2 and tide gauges', Remote Sens., vol. 11, no. 7, p. 744, Mar. 2019.
- [14] A. Richter, A. Groh, and R. Dietrich, 'Geodetic observation of sea-level change and crustal deformation in the Baltic Sea region', Phys. Chem. Earth, Parts A/B/C, vol. 53-54, pp. 43-53, Jan. 2012.
- [15] I. Varna, D. Haritonova, and J. Balodis, 'Velocity fields of the Latvian CORS station daily coordinates for 2012-2017', Geophysica, vol. 54, no. 1, pp. 137-144, 2019.
- [16] J. Balodis, I. Varna, D. Haritonova, and K. Morozova,

- 'Coordinate analysis of Latvian CORS stadions', Balt. J. Mod. Comput., vol. 7, no. 4, pp. 513-524, 2019.
- [17] S. D. P. Williams, 'The effect of coloured noise on the uncertainties of rates estimated from geodetic time series', J. Geod., vol. 76, no. 9-10, pp. 483-494, Feb. 2003.
- [18] M. S. Bos, R. M. S. Fernandes, S. D. P. Williams, and L. Bastos, 'Fast error analysis of continuous GPS observations', J. Geod., vol. 82, no. 3, pp. 157-166, Mar. 2008.
- [19] J. Langbein, 'Estimating rate uncertainty with maximum likelihood: Differences between power-law and flicker-random-walk models', J. Geod., vol. 86, no. 9, pp. 775-783, 2012.
- [20] S. D. P. Williams, 'CATS: GPS coordinate time series analysis software', GPS Solut., vol. 12, no. 2, pp. 147-153, Mar. 2008.
- [21] A. Mao, C. G. A. Harrison, and T. H. Dixon, 'Noise in GPS coordinate time series', J. Geophys. Res. Solid Earth, vol. 104, no. B2, pp. 2797-2816, Feb. 1999.
- [22] K. Dmitrieva, P. Segall, and C. DeMets, 'Network-based estimation of time-dependent noise in GPS position time series', J. Geod., vol. 89, no. 6, pp. 591-606, 2015.
- [23] Z. Malkin and A. V. Voinov, 'Preliminary results of processing EUREF network observations using a non-fiducial strategy', Phys. Chem. Earth, Part A Solid Earth Geod., vol. 26, no. 6-8, pp. 579-583, 2001.
- [24] X. Niu et al., 'Using Allan variance to analyze the error characteristics of GNSS positioning', GPS Solut., vol. 18, no. 2, pp. 231-242, 2014.
- [25] M. Hackl, R. Malservisi, U. Hugentobler, and R. Wonnacott, 'Estimation of velocity uncertainties from GPS time series: Examples from the analysis of the South African TrigNet network', J. Geophys. Res. Solid Earth, vol. 116, no. 11, pp. 1-12, 2011.
- [26] C. Xu and D. Yue, 'Characterizing noise in daily GPS position time series with overlapping Hadamard variance and maximum likelihood estimation', Surv. Rev., vol. 49, no. 355, pp. 239-248, Jul. 2017.
- [27] T. Herring, 'MATLAB Tools for viewing GPS velocities and time series', GPS Solut., vol. 7, no. 3, pp. 194-199, Dec. 2003.
- [28] X. He et al., 'Review of current GPS methodologies for producing accurate time series and their error sources', J. Geodyn., vol. 106, pp. 12-29, May 2017.
- [29] D. W. Allan and J. A. Barnes, 'A modified "Allan variance" with increased oscillator characterization ability', in Thirty Fifth Annual Frequency Control Symposium, 1981, pp. 470-475.
- [30] W. J. Riley, Handbook of Frequency Stability Analysis, vol. 31, no. 1, 2008.
- [31] S. T. Dawkins, J. J. McFerran, and A. N. Luiten, 'Considerations on the measurement of the stability of oscillators with frequency counters', IEEE Trans. Ultrason. Ferroelectr. Freq. Control, vol. 54, no. 5, pp. 918-925, May 2007.
- [32] Z. Malkin, 'Study of astronomical and geodetic series using the Allan variance', Kinemat. Phys. Celest. Bodies, vol. 27, no. 1, pp. 42-49, Feb. 2011.
- [33] G. Blewitt, W. Hammond, and C. Kreemer, 'Harnessing the GPS Data Explosion for Interdisciplinary Science', Eos (Washington DC), vol. 99, Sep. 2018.
- [34] R. Dach, S. Lutz, P. Walser, and P. Fridez, Bernese GNSS Software Version 5.2, vol. 47, no. November, 2015.
- [35] Z. Altamimi, 'EUREF Technical Note 1: Relationship and transformation between the international and the European

- terrestrial reference systems', in EUREF Technical Note 1: Version June 28, 2018, 2018, p. 11.
- [36] G. A. Milne, 'Space-geodetic constraints on glacial isostatic adjustment in Fennoscandia', Science, vol. 291, no. 5512, pp. 2381-2385, Mar. 2001.
- [37] O. Vestøl, J. Ågren, H. Steffen, H. Kierulf, and L. Tarasov, 'NKG2016LU: a new land uplift model for Fennoscandia and the Baltic Region', J. Geod., 93, no. 9, pp. 1759-1779, Sep. 2019.
- [38] G. Blewitt, C. Kreemer, W. C. Hammond, and J. Gazeaux, 'MIDAS robust trend estimator for accurate GPS station velocities without step detection', J. Geophys. Res. Solid Earth, vol. 121, no. 3, pp. 2054–2068, Mar. 2016.